Advances in Applied Mathematics and Mechanics
Adv. Appl. Math. Mech., Vol. **9**, No. 5, pp. 1052-1075

DOI: 10.4208/aamm.2015.m1283
October 2017

A Sharp Interface Method for Compressible Multi-Phase Flows Based on the Cut Cell and Ghost Fluid Methods

Xiao Bai[1,2] and Xiaolong Deng[2,*]

[1] *School of Mathematical Sciences, University of Science and Technology of China, Hefei, Anhui 230026, China*
[2] *Building 9, East Zone, ZPark II, No. 10 East Xibeiwang Road, Haidian District, Beijing Computational Science Research Center, Beijing 100193, China*

Received 9 September 2015; Accepted (in revised version) 20 April 2016

Abstract. A new sharp interface method with the combination of Ghost Fluid Method (GFM) and Cut Cell scheme is developed to study compressible multi-phase flows with clear interfaces. Straight-line cutting is applied on the cells passed by the interface. A new real-ghost mixing method is presented and applied around the cut cells to deal with very small cut cells. A cut face reconstruction method similar to volume of fluid is applied to deal with topological change problems. A high order Level Set (LS) method is applied to evolve the free interface, with the Level Set velocities from exact Riemann solver on the cut faces. Various 1D and 2D numerical examples are tested to show the robustness and ability of the present method in wide flow variable domains. This method benefits from cut cell on the sharp interface description, shows good conservation performance, and does not have the topological change difficulty of the full cut cell method presented in Chang, Deng & Theofanous, J. Comput. Phys., 242 (2013), pp. 946–990.

AMS subject classifications: 65M10, 78A48

Key words: Compressible multi-phase flows, cut cell method, level set method, ghost fluid method, interfacial dynamics.

1 Introduction

During the last decades, various numerical methods have been presented to study the dynamics of compressible multi-phase flows with clear material interfaces. In Lagrangian framework, a free interface can be tracked by mesh faces so that it can be dealt with sharply. But Lagrangian schemes have difficulty when the interface deforms strongly.

*Corresponding author.
Email: baixiao@csrc.ac.cn (X. Bai), xiaolong.deng@csrc.ac.cn (X. L. Deng)

 ©2017 Global Science Press

https://doi.org/10.4208/aamm.2015.m1283 Published online by Cambridge University Press

In Eulerian framework, a free interface needs to be captured/tracked by special methods, including Volume of Fluid [1, 2], Level Set [3–6], Phase Field [7, 8] method, Front Tracking [9, 10], Cut Cell [11, 12] et al..

In these numerical methods, how to deal with the jump conditions on the free interface is the key of getting good results. As a simple but effective way, several Ghost Fluid methods (GFMs) [13–19] have been presented. GFMs can be combined with different interface capturing/tracking methods. However, due to the existence of ghost fluid and ghost cells, the flow conservation may be not kept well near the interface, and the discontinuity position may be not captured very accurately. Hu et al. [20] presented a conservative interface method for compressible flows based on LS method, in which the concept of cut cell is applied and a mixing procedure is used to deal with small cells. Nourgaliev et al. [11] presented a cut cell method to deal with incompressible interfacial instabilities. Chang et al. [12] presented a consistent, conservative, all-speed sharp interfacial method, in which curved cut faces and unstructured mesh are generated by a cut cell scheme, and a merging scheme is applied to eliminate very small cells. With the realization of cut cell and curved cut faces, high accuracy is achieved, jump conditions are fully satisfied, and high density/pressure/viscosity ratio, strong surface tension, and strong acoustic-impedance mismatch can be handled naturally. However, topological change cannot be dealt with yet in this scheme due to the difficulty of handling multi-cut in one cell.

In this paper, we are considering the two-phase flow problems governed by the Euler equations. A real-ghost mixing method is presented, which helps to deal with the small cells cut by the cut faces, and makes the reconstruction and value update on the cells passed by the interface uniformly with the regular cells. A cut face reconstruction similar to volume of fluid is applied to solve the topological change difficulty of the full cut cell method presented in Chang et al. [12]. Together with the straight-line cutting method, high order LS method, and GFMs, a new sharp interface method is realized. Various 1D and 2D test cases show that this method can be widely applied in the compressible multi-phase problems with or without topological change accurately and robustly.

The remainder of this paper is organized as follows. In Section 2, a detailed description of the numerical implementation of the method is given. In Section 3, a set of numerical examples are presented to illustrate the feasibility and robustness of the proposed method. Finally, concluding remarks are given in Section 4.

2 Numerical methods

2.1 Infrastructure

In this work, the background mesh is structured, and some numerical schemes for unstructured mesh are applied near the material interface, around which cut cells and ghost cells are generated. Finite volume method is applied, with AUSM$^+$-up [21, 22] scheme to calculate the fluxes on the regular faces, and exact Riemann solver [12, 22] on the cut

https://doi.org/10.4208/aamm.2015.m1283 Published online by Cambridge University Press

faces. Time step is advanced by the four-stage Runge-Kutta method [23,24].

2.2 Basic equations

In this work, Euler equations are applied in conservation form:

$$\frac{\partial}{\partial t}\int_V W dV + \oint_S F dS = 0, \tag{2.1}$$

where

$$W = \begin{pmatrix} \rho \\ \rho \mathbf{v} \\ \rho E \end{pmatrix}, \qquad F = \begin{pmatrix} \rho U_n \\ \rho \mathbf{v} U_n + p\mathbf{n} \\ \rho E U_n + (p\mathbf{n})\cdot \mathbf{v} \end{pmatrix}.$$

$U_n = \mathbf{v}\cdot\mathbf{n}$, $\mathbf{v}$ is the velocity of fluid, $\mathbf{n}$ is the unit outward normal vector, ρ is fluid density, $E = e + \frac{1}{2}|\mathbf{v}|^2$ is the total specific energy, p is pressure, e is specific internal energy, T is temperature. The equation of state applied here is the stiffened-gas model

$$p = \frac{\gamma - 1}{\gamma} C_p \rho T - P_\infty, \qquad e = \frac{C_p}{\gamma} T + \frac{P_\infty}{\rho}. \tag{2.2}$$

2.3 Interface treatment

2.3.1 Level Set function

The free interface is evolved with the help of LS equation [3]

$$\frac{\partial \varphi}{\partial t} + \mathbf{v}_\varphi \cdot \nabla \varphi = 0. \tag{2.3}$$

Here, φ is LS function, which is originally defined as signed distance function to the material interface, and the zero value position of φ is the interface position. $\mathbf{v}_\varphi$ is the nearest interfacial velocity. The Eq. (2.3) is discretized by the HOUC3 format [25] and advanced in time by four-stage Runge-Kutta method. Both φ and $\mathbf{v}_\varphi$ are defined on the grid points. The value of $\mathbf{v}_\varphi$ in the vicinity of free interface is normally set to be equal to the nearest interfacial velocity, which is calculated by exact two-phase Riemann solver [12]. This is the way to keep signed distance property of the calculated LS values near the interface [26]. Around the topological change position, to avoid the problem coming from too close interfaces, it is equal to the velocity of local flow field. For the rest of domain, $\mathbf{v}_\varphi$ is obtained by the advancing-front propagating function [12]. When the re-initialization [27–29] is needed, the Eq. (2.4) is solved to steady state:

$$\frac{\partial \varphi}{\partial \tau} + S(\varphi_0)(|\nabla \varphi| - 1) = 0. \tag{2.4}$$

https://doi.org/10.4208/aamm.2015.m1283 Published online by Cambridge University Press

Here, τ is pseudo time, and the speed function $S(\varphi_0)$ is defined as

$$S(\varphi_0)=\begin{cases} -1, & \varphi_0<0, \\ 0, & \varphi_0=0, \\ 1, & \varphi_0>0. \end{cases} \tag{2.5}$$

In implementation, we use

$$S(\varphi_0)=S(\varphi,\varphi_0)=\frac{\varphi}{\sqrt{\varphi^2+|D\varphi|^2\Delta x^2}}|2H(\varphi_0)-1|$$

from [30],

$$H(\varphi_0)=\begin{cases} 0, & \varphi_0<-\epsilon, \\ \frac{1}{2}\Big[1+\frac{\varphi_0}{\epsilon}+\frac{1}{\pi}\sin\Big(\frac{\pi\varphi_0}{\epsilon}\Big)\Big], & |\varphi_0|\le\epsilon, \\ 1, & \varphi_0>\epsilon. \end{cases} \tag{2.6}$$

Here ϵ is a small number, normally set to be $2.5\Delta x$ in our simulations. The method presented by Sussman et al. [28] is used to solve it.

2.3.2 Cut Cell computation

In cut cell method, when a mesh cell is passed across by a material interface, it can be separated to smaller cells, which are called cut cells. The material interface is then represented by piecewise cut faces in this scheme. The intersection points of the mesh faces and the material interface are called cut points. The resulted cut cells can be very small so that the time step needs to be very small due to the limit of CFL condition. A real-ghost mixing method is presented to solve this problem so that the time step is calculated only based on the standard cell size. In this mixing method, a cut cell on one side of the cut face is also a ghost cell of the other side, and the ghost fluid state is calculated by suitable GFM.

Fig. 1 shows the basic structure of cut cell, cut face and ghost cell. When the fluid state of standard cell (i,j) is required in the reconstruction scheme for Fluid1, the values in CC1 and GC1 in (i,j) will be mixed by averaging weighted by volumes of cut cells. When the cell $(i+1,j)$ is required for Fluid1 calculation, simply the GC1 values in $(i+1,j)$ are used. In this way, the reconstruction scheme can be implemented uniformly.

The level set function φ is defined at the cell vertices, and the cut points can be identified by the level set values. For example, if the cell vertices $(x_{i,j},y_{i,j})$ and $(x_{i+1,j},y_{i,j})$ have opposite sign level set values $\varphi_{i,j}$ (>0) and $\varphi_{i+1,j}$ (<0), then the cut point coordinate can be given by a simple linear interpolation, which is $((|\varphi_{i,j}|x_{i+1,j}+|\varphi_{i+1,j}|x_{i,j})/(|\varphi_{i,j}|+|\varphi_{i+1,j}|),y_{i,j})$. Then the geometrical quantities (such as volume, centroid, unit normal vector) of a cut cell or a cut face are calculated by the analytic geometry method. The state of a cut cell is evolved in time, and the state on either side of a cut face is obtained by the least-square reconstruction method. Besides, the volume fraction on a cut cell is calculated with a direct geometry calculation.

https://doi.org/10.4208/aamm.2015.m1283 Published online by Cambridge University Press

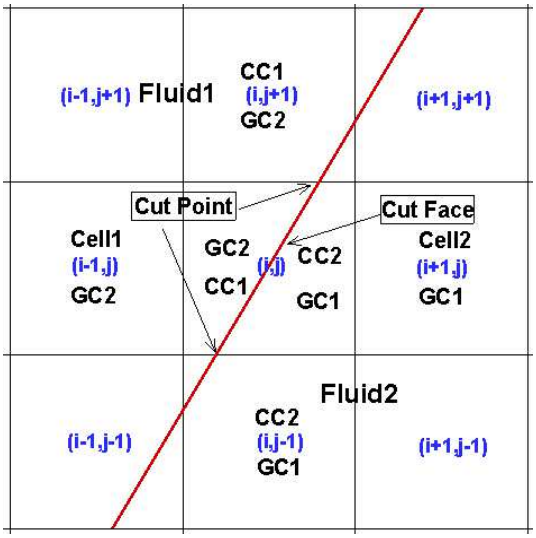


Figure 1: Diagram of cell, cut cell, cut face, cut point and ghost cell. All smaller cells cut from the mother whole cells are called cut cells; the red faces are called cut faces. Ghost cells are constructed on cut cells and the whole cells near the interface. "CC" means "cut cell", "GC" means "ghost cell", and the numbers after them are fluid index.

The state of ghost fluid is obtained by the OGFM [13] for gas-gas, and the GWGFM [14, 15] for air-water cases. Due to the existence of cut face, it is quite convenient to calculate interfacial normal vector, which are important for the implementation of the GFMs.

When a cell is passed by the interface for more than once, the topological change is about to occur. The concept of Volume of Fluid method is applied to reconstruct a cut face to keep the volume fraction to be same, and the normal vector of the new cut face is simply determined by Youngs' finite-difference method [31,32]. For example, the cell (i,j) in Fig. 2 is cut twice and **Fluid1** in this cell is separated into two parts by the material interface, the volume fraction(α) of **Fluid1** in every cell is known and the normal vector of the new cut face is estimated as a gradient, $\mathbf{n}=-\nabla\alpha/|\nabla\alpha|$. Here, $\mathbf{n}=(n_x,n_y)=(N_x/\sqrt{N_x\cdot N_x+N_y\cdot N_y},N_y/\sqrt{N_x\cdot N_x+N_y\cdot N_y})$, and

$$N_x=-1/8(\alpha_{i+1,j+1}+2\alpha_{i+1,j}+\alpha_{i+1,j-1}-\alpha_{i-1,j+1}-2\alpha_{i-1,j}-\alpha_{i-1,j-1}), \tag{2.7a}$$

$$N_y=-1/8(\alpha_{i+1,j+1}+2\alpha_{i,j+1}+\alpha_{i-1,j+1}-\alpha_{i+1,j-1}-2\alpha_{i,j-1}-\alpha_{i-1,j-1}). \tag{2.7b}$$

In this way, the merging and separation of the interface is simply treated.

2.3.3 Cut Cell update

In each time step, after the computation of the state and geometrical quantities of cut cells and ghost cells, the fluid state quantities of a cut cell in the next time step are updated as follows. For simplicity, here the process is illustrated by only considering **Fluid1**, and it is similar for **Fluid2**. First, a mixing state quantity for **Fluid1** is obtained by combining the cut cell and corresponding ghost fluid state, as shown in Fig. 3, the mixing

https://doi.org/10.4208/aamm.2015.m1283 Published online by Cambridge University Press

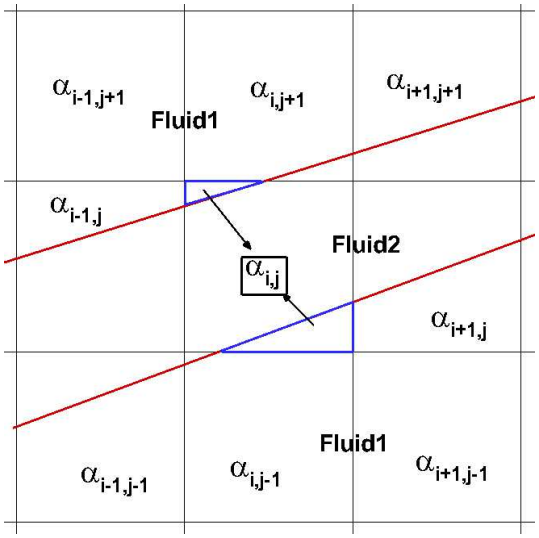


Figure 2: Diagram of volume fraction of **Fluid1** and multiple cuts. The α is volume fraction of **Fluid1**, and the two red lines represent the material interfaces. Here, a cell is cut twice and the $\alpha_{i,j}$ is total volume fraction of **Fluid1** in the cell (i,j).

state $\mathbf{W}_{i,j}^{mix}=\alpha_{i,j}\mathbf{W}_{i,j}^{CC1}+(1-\alpha_{i,j})\mathbf{W}_{i,j}^{GC1}$. Then the mesh interface states are calculated by MUSCL scheme. For example, the mesh interface state quantities $\mathbf{F1}_{i,j}^{R}$ and $\mathbf{F1}_{i+1,j}^{L}$ are reconstructed with the three cell states $(\mathbf{W}_{i-1,j},\mathbf{W}_{i,j}^{mix},\mathbf{W}_{i+1,j}^{GC1})$. And the mesh interface fluxes are obtained by the AUSM^{+}-up scheme [22]. At last, the cell state $\mathbf{W}_{i,j}^{n+1}$ in the next time step is obtained in the explicit finite volume way, and is given to the new cut cell from updated Level Set values, as $\mathbf{W}_{i,j}^{CC1,n+1}$. In this way, the cut cell state for each fluid is updated. We call the real and ghost cut cells arrangement, the mixing process for reconstruction and the cut cell state update process together the real-ghost mixing method, which helps to calculate cut cell state values without very small time step problem from very small cut cells.

2.4 Time integration and solution procedure

First, with space discretization, Eq. (2.1) becomes:

$$\frac{\partial}{\partial t}(WV)+\sum_{m}(F_iS_i)=0. \tag{2.8}$$

Here, V is the volume of a cell, m is the total number of faces of the cell, which is 4 for a 2D regular cell. Then we use the four-stage Runge-Kutta method to advance the solution

https://doi.org/10.4208/aamm.2015.m1283 Published online by Cambridge University Press

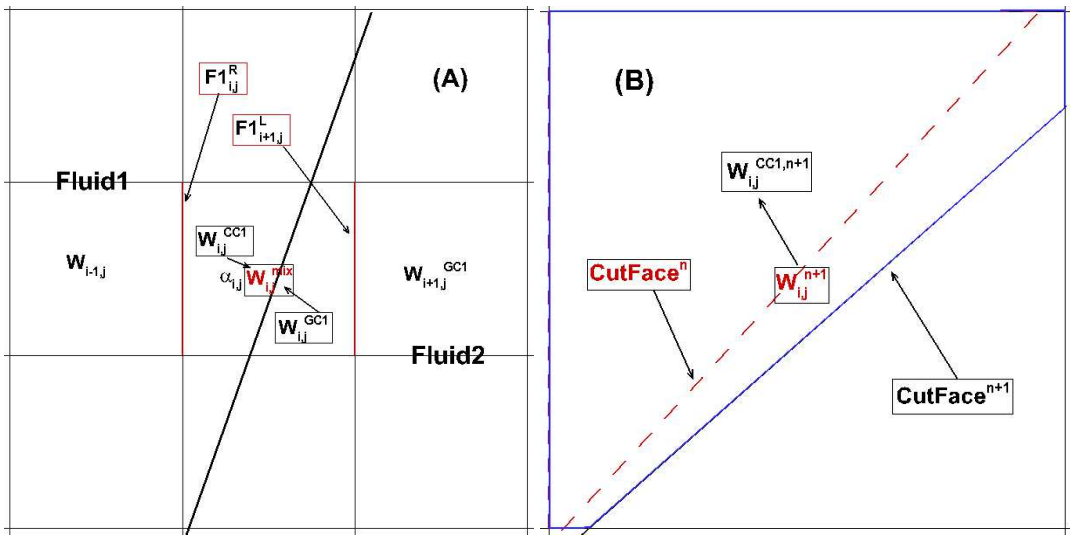


Figure 3: State quantities update of cut cell. (A) shows the mixing state ($\mathbf{W}_{i,j}^{mix}$) of cut cell ($\mathbf{W}_{i,j}^{CC1}$) and corresponding ghost cell ($\mathbf{W}_{i,j}^{GC1}$), and the mesh interface state ($\mathbf{F1}_{i,j}^{R}$,$\mathbf{F1}_{i+1,j}^{L}$), the volume fraction of cut cell for **Fluid1** $\alpha_{i,j}$. Besides, the whole cell state and whole ghost cell state are given by $\mathbf{W}_{i-1,j}$, $\mathbf{W}_{i+1,j}^{GC1}$, respectively. (B) shows the update of cut cell. **CutFace**^{n} and **CutFace**$^{n+1}$ denote the cut face at n-time and $(n+1)$-time, respectively. $\mathbf{W}_{i,j}^{n+1}$ denotes the updated mixing state of **Fluid1**, and $\mathbf{W}_{i,j}^{CC1,n+1}$ is the new cut cell state of **Fluid1**.

in time,

$$W^{(1)}V^{(1)} = W^nV^n - \omega_1\Delta t\sum_m (F_i^nS_i^n), \tag{2.9a}$$

$$W^{(2)}V^{(2)} = W^nV^n - \omega_2\Delta t\sum_m (F_i^{(1)}S_i^{(1)}), \tag{2.9b}$$

$$W^{(3)}V^{(3)} = W^nV^n - \omega_3\Delta t\sum_m (F_i^{(2)}S_i^{(2)}), \tag{2.9c}$$

$$W^{n+1}V^{n+1} = W^nV^n - \omega_4\Delta t\sum_m (F_i^{(3)}S_i^{(3)}), \tag{2.9d}$$

where $(\omega_1,\omega_2,\omega_3,\omega_4) = (1/4,1/3,1/2,1)$.

The general procedure of the current method can be summarized as follows:

1. Initially calculate the LS values of cells and vertices. From the LS values of vertices, get cut points, cut faces and cut cells, compute the geometrical quantities of cut cells and cut faces, and volume fractions of cells. Give the state quantities of cells, cut cells and vertices.

2. Reconstruct the states on cut faces, calculate the normal velocities and pressures on cut faces with the exact Riemann solver.

https://doi.org/10.4208/aamm.2015.m1283 Published online by Cambridge University Press

3. Calculate the states of ghost cells.
4. Reconstruct the states of regular faces, then obtain the numerical fluxes at these faces by the approximate Riemann solver AUSM$^+$-up.
5. Calculate velocities $\mathbf{v}_\varphi$ at vertices in the vicinity of interface and propagate them to all the other vertices.
6. Update the LS values on vertices by HOUC3 method, re-initialize the LS values if needed.
7. Update cut cells and cut faces, calculate the geometrical quantities, and obtain the new volume fractions of cells.
8. Update the state quantities of cells, cut cells, and calculate the state quantities on vertices.
9. go to 2 for the next step.

3 Numerical examples

In this section, numerical examples are presented to demonstrate the performance of the proposed method. For the 1D examples, the computational domain is 10m $\times$ 1m, space resolution is 100 grids/m; the upper and lower boundaries are imposed with symmetrical boundary condition, and the left and right boundaries imposed with inflow and outflow boundary conditions. In 2D cases, boundary conditions are different and given for each case. All the computations are carried out with the CFL number of 0.4 or 0.2.

3.1 1D shock tube problems

Case A (gas-gas): As the first numerical test, we consider a well known air-helium shock tube problem [19, 20] in rectangular domain [-5m,5m]$\times$[0m,1m], and the interface is located at x=0m. the state parameters are: γ_{Air}=1.4, $C_{p,Air}$=1004.85J/(kg$\cdot$ K); γ_{Helium}=1.63, $C_{p,Helium}$=5353.65J/(kg$\cdot$ K). The initial conditions are as follows:

$$(\rho,p,u,T)_{Air} = (2.282g/l,2.56bar,246.6m/s,390.4K), \tag{3.1a}$$
$$(\rho,p,u,T)_{Helium} = (0.167g/l,1.01bar,0m/s,293.15K). \tag{3.1b}$$

The analytical solution for this problem consists of the transmitted shock moving to the right, and the rarefaction wave moving to the left, as shown in Fig. 4. This result is after 2000 time steps, at $t = 2.29$ms. The numerical results agree with the exact solution very well. A sharp density jump can be seen at material interface in the density plot due to the cut cell method used in this paper.

https://doi.org/10.4208/aamm.2015.m1283 Published online by Cambridge University Press

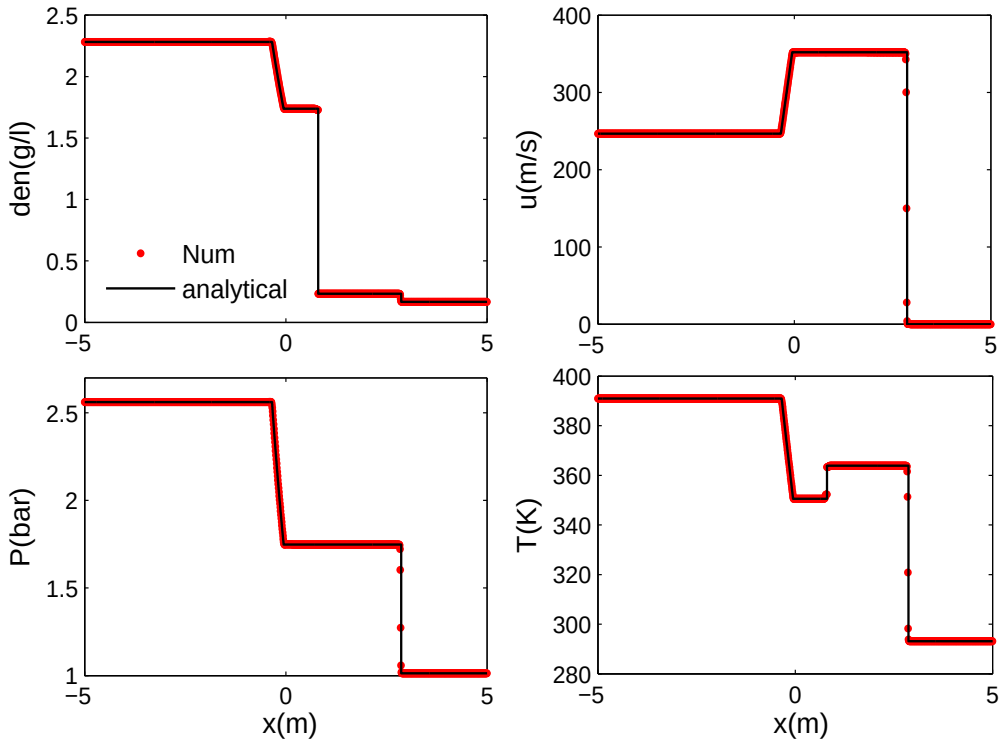


Figure 4: Air-Helium test case: comparison between numerical solution and analytical solution. $\Delta x = 0.01$, $t = 2.29$ms.

The next test is about Air-SF_6 shock tube problem. The reason we choose this case is that it makes a two-shock propagation. The state parameters are: $\gamma_{Air} = 1.4$, $C_{p,Air} = 1004.85\text{J}/(\text{kg}\cdot\text{K})$; $\gamma_{SF_6} = 1.093$, $C_{p,SF_6} = 669.48\text{J}/(\text{kg}\cdot\text{K})$. And the initial conditions are:

$$(\rho,p,u,T)_{Air} = (1.59g/l, 1.51bar, 104.89m/s, 330.67K), \tag{3.2a}$$
$$(\rho,p,u,T)_{SF_6} = (5.99g/l, 1.0bar, 0m/s, 293.15K). \tag{3.2b}$$

Other conditions are the same with the above Air-Helium case. After 2000 time steps, at $t = 8.525$ms, the numerical results are shown in Fig. 5. For this problem, there are two shock waves moving to the left in air and to the right in SF_6. As shown in Fig. 5, the numerical results agree with the analytical solution very well.

Case B (Air-Water): The gas-liquid shock tube problem is introduced by Saurel and Abgrall [33]. The equation of state for water is stiffen-gas equation of state. The state parameters are: $\gamma_{Air} = 1.4$, $C_{p,Air} = 1004.85\ \text{J}/(\text{kg}\cdot\text{K})$, $P_\infty = 0.0$ Pa for air; $\gamma_{Water} = 2.788103$, $C_{p,Water} = 4190.00\text{J}/(\text{kg}\cdot\text{K})$, $P_\infty = 7.862511\times10^8$Pa for water. The initial conditions are:

$$(\rho,p,u,T)_{Water} = (1499.77g/l, 2.0GPa, 818.52m/s, 691.35K), \tag{3.3a}$$
$$(\rho,p,u,T)_{Air} = (1.224g/l, 1.03bar, 0m/s, 293.15K). \tag{3.3b}$$

https://doi.org/10.4208/aamm.2015.m1283 Published online by Cambridge University Press

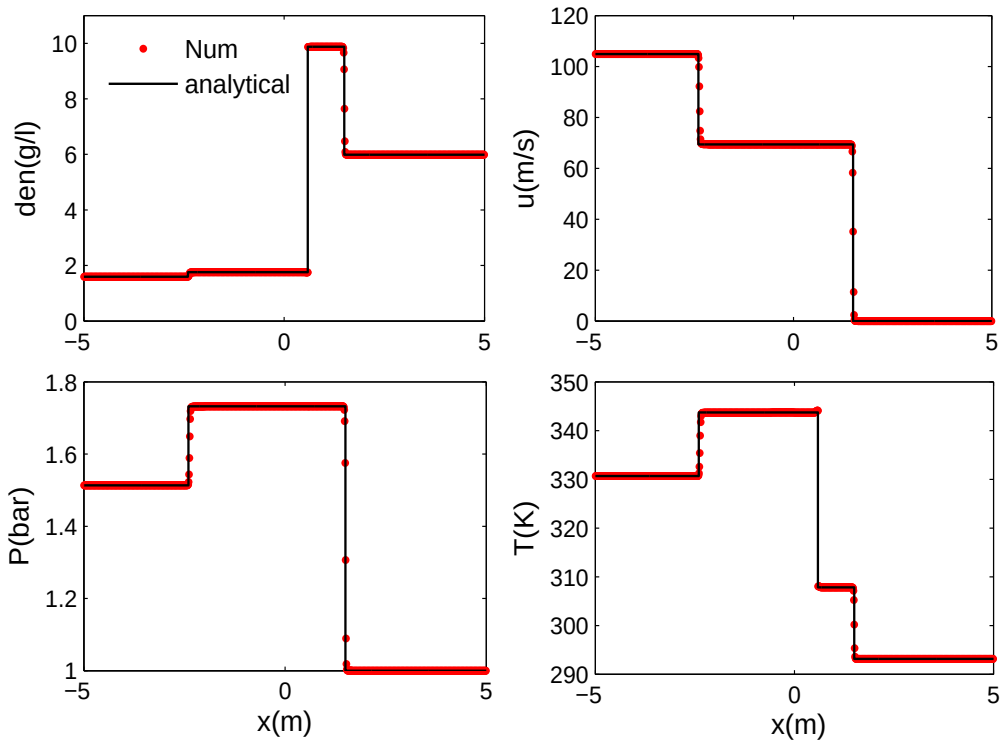


Figure 5: Air-SF_6 test case: comparison between numerical solution and analytical solution. $\Delta x = 0.01$, $t =$ 8.525ms.

Other conditions are same with the above gas-gas cases. After 3500 time steps, at $t =$ 2.167ms, the numerical results are shown in Fig. 6. Fig. 6 shows good agreement between the numerical results and the analytical solution.

The 1D test cases show that current method can effectively deal with the shock tube problems including gas-gas and gas-liquid cases. In a wide range of density ratio and shock strength, this method gives good results. In the next subsection, some 2D cases are tested.

3.2 Single-mode Richtmyer-Meshkov instability in 2D

The Richtmyer-Meshkov instability (RMI) was originally presented by Richtmyer [34] and Meshkov [35,36]. Holmes [37,38]) and Ullah et al. [39] presented some good numerical results using Front-Tracking methods. In our previous work, this problem has been considered with MuSiC$^+$ code based on the full cut cell method [12], but that is hard to deal with topological changes. Here two cases of RMI are tested. One is Air-SF_6; the other is the Air-Helium that contains phase reversal phenomenon. The Air-SF_6 case is set in the computational domain [0m, 5m]$\times$ [0m, 1m], and the boundary conditions are symmetric

https://doi.org/10.4208/aamm.2015.m1283 Published online by Cambridge University Press

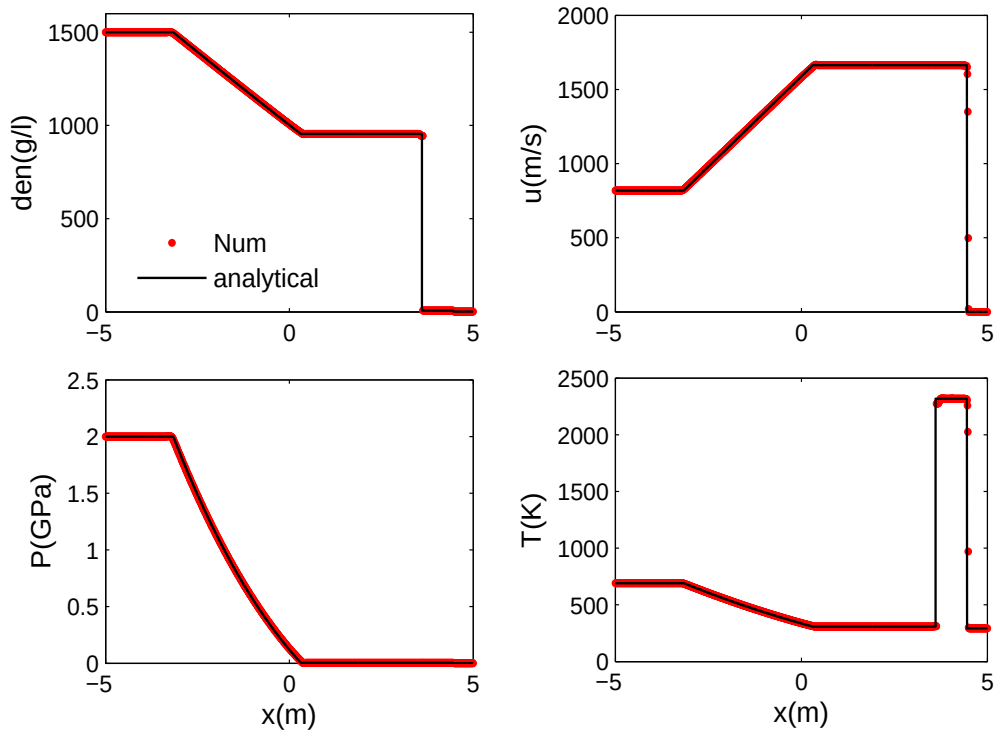


Figure 6: Water-Air test case: comparison between numerical solution and analytical solution. $\Delta x = 0.01$, $t = 2.167$ms.

in y-direction and inflow and outflow in x-direction. The initial interface is described as

$$x = x_I + \epsilon \cos\left(\frac{2\pi}{\lambda} y\right), \tag{3.4}$$

where $x_I = 1.1$m is the location of unperturbed interface, $\epsilon = 0.1$m is the amplitude of the imposed perturbation, $\lambda = 1$m is the wavelength. The state parameters are the same as those in the 1D Air-SF_6 shock tube case. A planar $M_{sh} = 1.24$ shock wave is placed in the air at $x = 0.8$m, with pre- and post-shock conditions:

$$(\rho, p, u, v)_{Preshock} = (1.20g/l, 1.01bar, 0m/s, 0m/s), \tag{3.5a}$$
$$(\rho, p, u, v)_{Postshock} = (1.698g/l, 1.65bar, 124.0m/s, 0m/s). \tag{3.5b}$$

Space resolution is 200 grids per λ. The density distribution at different time is shown in Fig. 7. When the incident shock hit the interface, a transmitted shock in SF_6 and a reflected shock in air appear, and the interface moves to the right, forming a bubble of air injected into SF_6 and a spike of SF_6 injected into air. Due to the initial perturbation of interface, there is a misalignment of pressure and density gradients which generates vorticity and then mushroom shape is formed, as seen in Fig. 7 at time $t = 203\mu$s. The

https://doi.org/10.4208/aamm.2015.m1283 Published online by Cambridge University Press

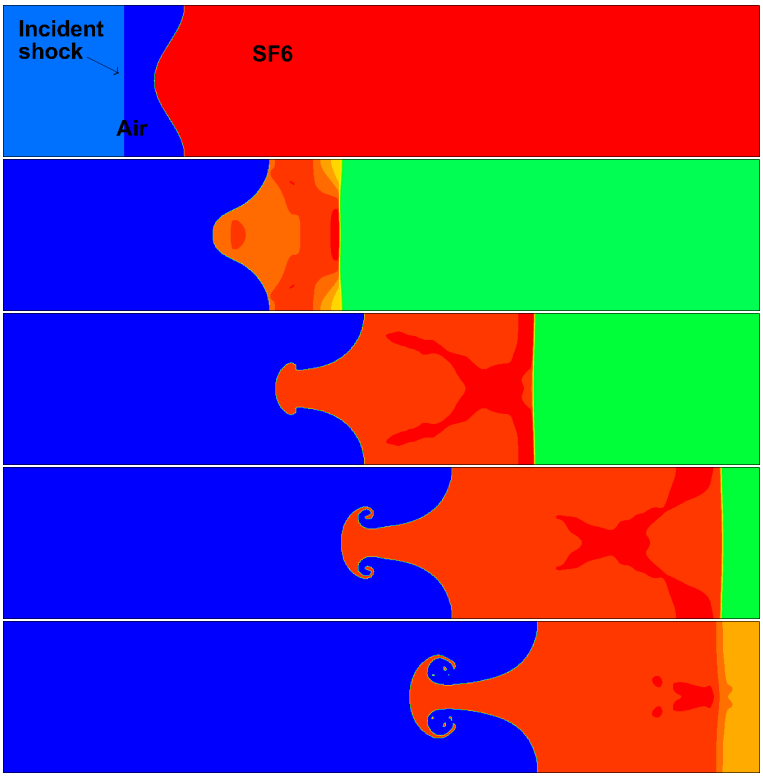


Figure 7: Air-SF_6 Richtmyer-Meshkov instability: dynamics of the interface and density field for numerical results at different times. Time from upper to lower is 0μs, 68μs, 136μs, 203μs, 270μs.

mushroom shape will separate and mix because of the effect of vorticity at time $t=270\mu$s. Current method treats the merging and separation process of material interface naturally.

Next, the interfacial instability of Air-Helium is tested in the computational domain [-10m, 30m]$\times$[0m, 4m]. The boundary conditions are the same as those in the Air-SF_6 case. The initial interface is also described by the Eq. (3.4), and $x_I=0.0$m, $\epsilon=0.2$m, $\lambda=4$m. The state parameters are the same as those in the 1D shock tube case of Air-Helium. A planar $M_{sh}=1.5$ shock wave is placed in the air at $x=-1.0$m, with pre- and post-shock conditions:

$$(\rho,p,u,v)_{Preshock}=(1.20g/l,1.01bar,0m/s,0m/s), \tag{3.6a}$$
$$(\rho,p,u,v)_{Postshock}=(2.28g/l,2.56bar,246.6m/s,0m/s). \tag{3.6b}$$

Space resolution is 200 grids per λ(wavelength). The density distribution at different time is provided in Fig. 8.

The mechanism is similar to Air-SF_6 case, but the phase will reverse due to the reversed density gradient. The interface moves from heavy to light gas, the bubble in air will become spike and the spike in helium will become bubble. The mushroom shape

https://doi.org/10.4208/aamm.2015.m1283 Published online by Cambridge University Press

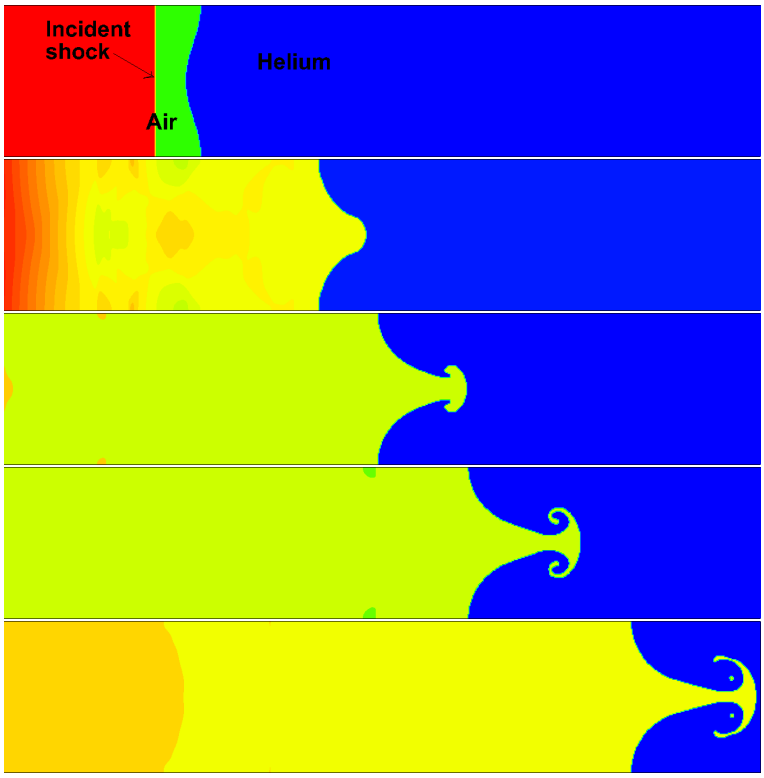


Figure 8: Air-Helium Richtmyer-Meshkov instability: dynamics of the interface and density field for numerical results at different times. Time from upper to lower is 0μs, 198μs, 395μs, 585μs, 782μs.

appears as shown in Fig. 8 at time $t=585\mu$s, similarly the interface will break up due to the effect of vorticity at time $t=782\mu$s. The evolution of interfacial shape is similar to the previous works [25,39,40].

3.3 Shock-bubble interaction

In this section, two famous cases of the shock-bubble interaction presented by Hass and Sturtevant [41] on experiments will be tested. The experiments were carried out in a horizontally placed shock tube with square section filled with air. A cylindrical bubble with diameter 5 cm was placed in the middle of the shock tube, filled with helium in the first experiment and R22 in the second one. A vertical planar weak shock with Mach number 1.22 is produced to the right of the bubbles, and moves towards the bubble. The set-up of the experiments is just as shown in Fig. 9, and the experimental parameters are presented in Table 1. Symmetric boundary conditions are used in y-direction, and inflow and outflow conditions are set in x-direction.

Next, the density contours of the Air-Helium and Air-R22 are considered at different times, and these results are also compared with experiment results in [41], and numerical

https://doi.org/10.4208/aamm.2015.m1283 Published online by Cambridge University Press

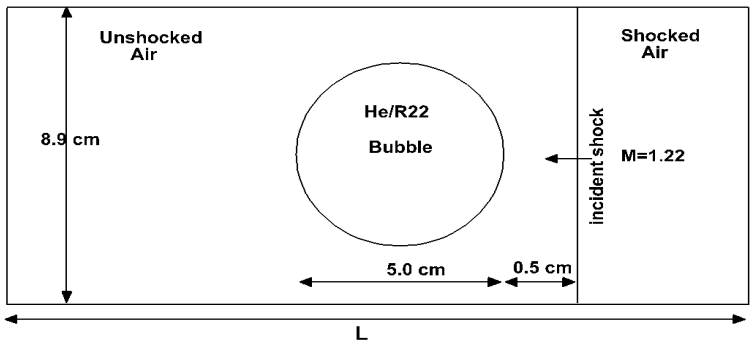


Figure 9: Initial set-up for shock-bubble interaction problems.

results presented by [42] and [43].

Fig. 10 shows that the present numerical results basically agree with the experiments [41] and other numerical results presented by [42] and [43]. The grid resolution in this case is 1000/8.9 grids per bubble dimater, same as that used in [43]. Some subtle difference may be observed at time 427μs or later, due to the evolution of interfacial instability. Vortices are then generated on the surface of helium bubble as shown in Fig. 10 at time 674μs, which is also observed in [43].

Air-R22 interaction is then tested. The set-up has been given above. The numerical results are also compared with experiments [41] and other numerical results [43, 44].

Fig. 11 shows that the numerical results with current method agree with the experiment results, and the numerical results in [44] and [43]. The vorticies called "Vortex

Table 1: Air-Helium/R22 bubble parameters [43].

Quantity	Units	Symbol	Value
Air-Helium			
Radius of helium bubble	cm	r_{bubble}	2.5
initial density	g/l	ρ_{air}	1.225
-	g/l	ρ_{helium}	0.2228
Initial pressure	bar	P	1.01325
Shock strength	Mach number	M	1.22
Ratio of specific heats	-	γ_{air}	1.4
-	-	γ_{helium}	1.648
Air-R22			
Radius of R22 bubble	cm	r_{bubble}	2.5
initial density	g/l	ρ_{air}	1.225
-	g/l	ρ_{R22}	3.8635
Initial pressure	bar	P	1.01325
Shock strength	Mach number	M	1.22
Ratio of specific heats	-	γ_{air}	1.4
-	-	γ_{R22}	1.249

https://doi.org/10.4208/aamm.2015.m1283 Published online by Cambridge University Press

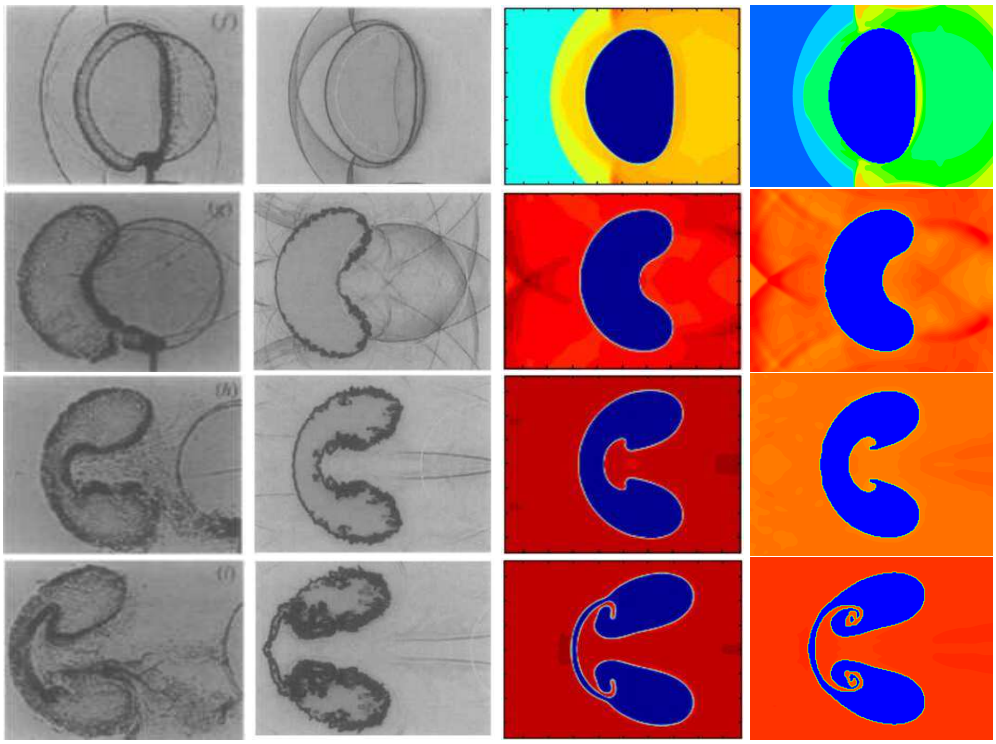


Figure 10: Air-Helium bubble interaction: comparison among experiments shadowgraphs (Haas & Sturtevant 1987 [41]) (left column), numerical schlieren images (Quirk et al. 1996 [42]) (left center column), numerical density contours (Ullah et al. 2013 [43]) (right center column), and the numerical results by current method (right column) at times: 102μs, 245μs, 427μs, 674μs, from top to bottom. Simulation times are corrected following [43].

head" can be seen at time 417μs and later. Due to Richtmyer-Meshkov (RM) and Kelvin-Helmholtz (KH) instabilities, the interface significantly deforms, sequentially breaks up into small pieces.

There are some differences among the three numerical simulations, especially at later times, which may be due to the numerical dissipations of different methods.

3.4 Collapse of 2D gas bubble under strong shock in water

The case of air bubble collapse induced by a strong shock in water has been simulated by many numerical methods including Front-Tracking methods [45, 46], Level Set methods [19, 30], and Volume of Fluid [47]. In this subsection, the experiments carried out by Bourne and Field [48] are considered. The set-ups are: a cylindrical air bubble with diameter 6mm is immersed in water. The center of bubble is located at $\mathbf{x}_c$ =(6mm , 6mm) in computational domain of size 12 $\times$ 12mm^2. A planar incident $M_{sh} = 1.72$ shock wave is initially located at 3.6mm to the left of the air bubble center. The grid resolution is

https://doi.org/10.4208/aamm.2015.m1283 Published online by Cambridge University Press

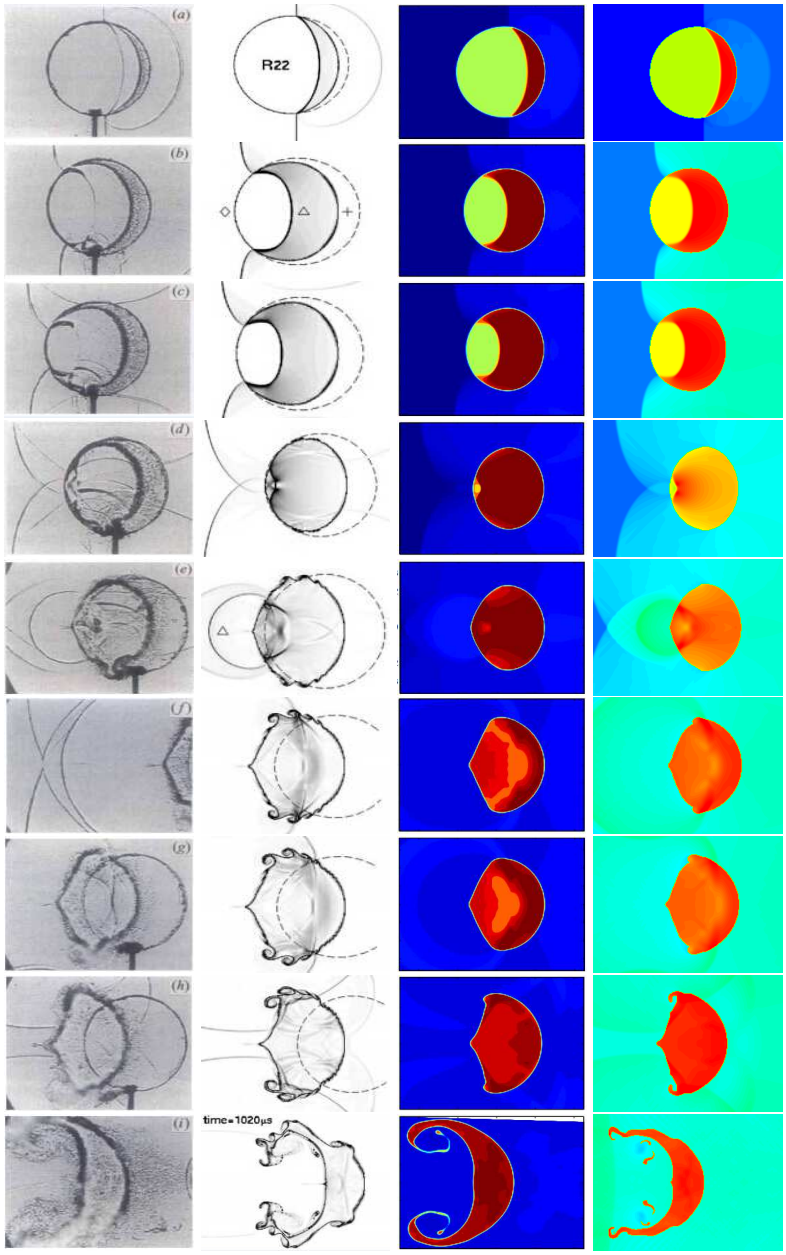


Figure 11: Air-R22 bubble interaction: comparison among experiments shadowgraphs (Haas & Sturtevant 1987 [41]) (left column), numerical density contours (Shyue et al. 2006 [44] (left center column), Ullah et al. 2013 [43] (right center column) and current results (right column)) at times: 55μs, 115μs, 135μs, 187μs, 247μs, 318μs, 342μs, 417μs and 1020μs, from top to bottom.

200 computational nodes per initial bubble's diameter. The parameters are: $\gamma = 4.4$, $P_\infty = 6.0\times10^8$Pa for water and $\gamma = 1.4$, $P_\infty = 0.0$Pa for air. Initial state: pre-shock: ve-

https://doi.org/10.4208/aamm.2015.m1283 Published online by Cambridge University Press

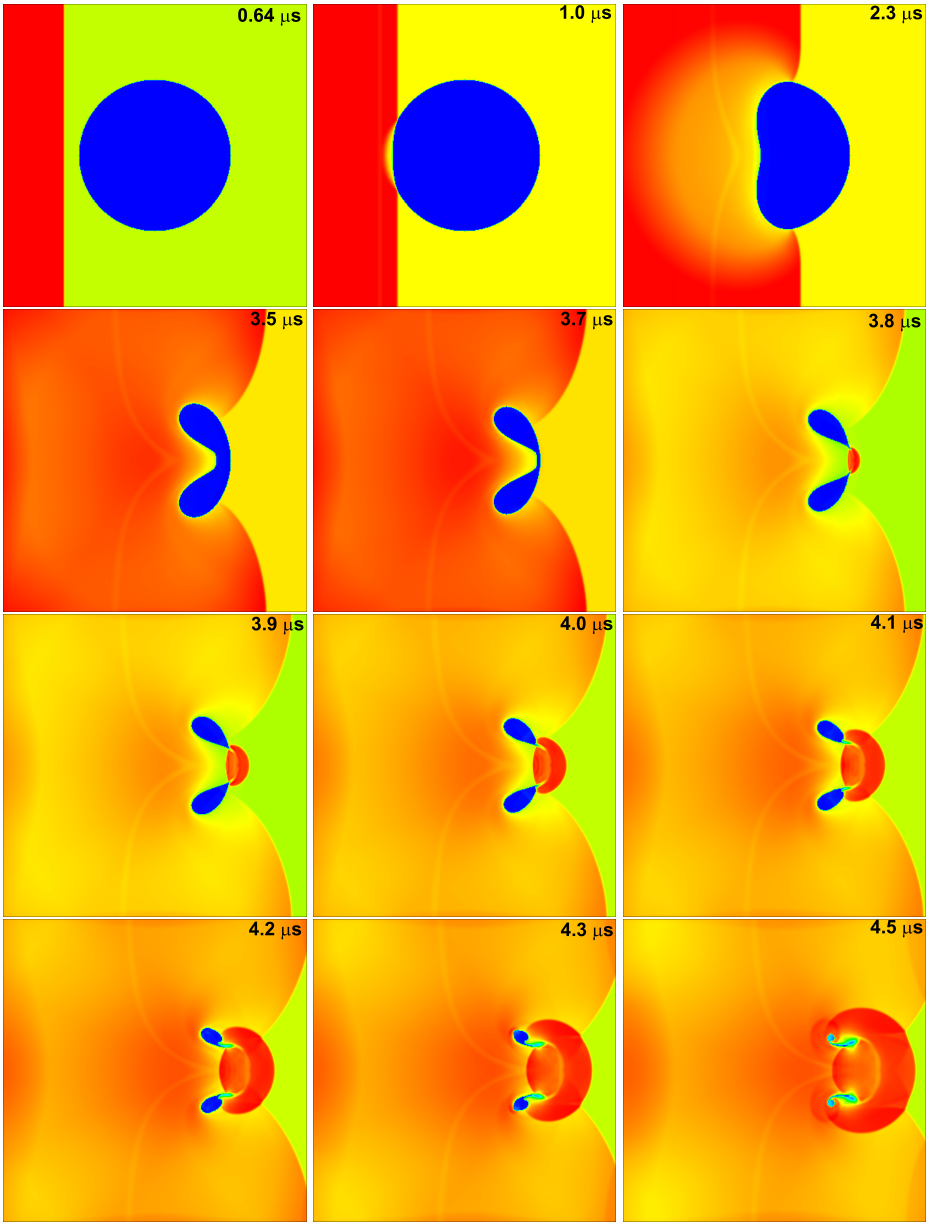


Figure 12: Evolution of the density field of underwater air bubble collapse case. Effective grid resolution is 200 cells per initial bubble diameter.

locity $\mathbf{u}=(0,0)\text{m/s}$, $P=1.03\times10^5\text{Pa}$, $\rho_{water}=998.23\text{g/l}$ and $\rho_{air}=1.22\text{g/l}$; post-shock: $\mathbf{u}=(685.86,0)\text{m/s}$, $P=1.915\text{GPa}$, $\rho_{water}=1322.47\text{g/l}$. The left boundary condition is inflow and others are outflow.

For the present case, the initial time is set to be $0.64\mu\text{s}$ in the previous cases [30,47,49].

https://doi.org/10.4208/aamm.2015.m1283 Published online by Cambridge University Press

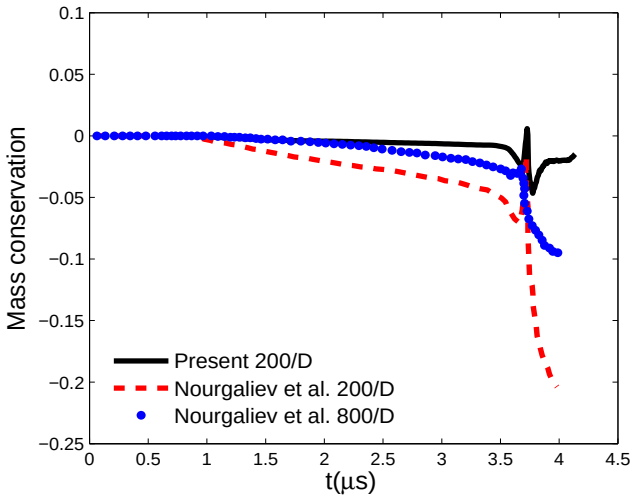


Figure 13: Mass conservation in the bubble collapse case. Black line is present result for 200/D, red line (200/D) and blue line (800/D) are from [30].

Fig. 12 shows that after hitting the bubble, a reflected rarefaction wave are generated in water and an incident shock transmits into bubble. A water jet is generated at about 2.3μs, and hits the other side of air bubble with velocity 2837m/s at about 3.7μs. Then the bubble breaks up into two pieces, and a blast wave appears at about 3.8μs. The second jets appear due to the interaction between the blast wave and the two lobes at about 4.1μs and later, and at about 4.5μs the maximum temperature is about 25000K in air bubble. Current results are consistent with those of the previous works.

Most LS methods do not keep mass conservation, so is this method. But it still shows good conservation behavior. Fig. 13 shows that the mass loss of current method is quite lower than that of the LS method applied in [30]. In this method, the interface is obtained by cut cell method, which can separate respective fluids sharply and explicitly. This is why this method shows better conservation than [30], even with much coarser grids, as shown in Fig. 13.

3.5 Underwater explosion

Underwater explosion problem has been considered in [22, 30, 49–52]. Two points are focused in this test: one is the interaction between the bubble and material interface of ambient water and air; the other is mixing between the air bubble and ambient air. Initial condition: an air bubble with high pressure (1.0GPa) and density (1250g/l) is located at (2.0m, 1.2m) in domain [0m, 4m]$\times$[0m, 4m]; the bubble diameter is 0.24m and the material interface is located at $y=1.5$m. The normal temperature and pressure is applied in the ambient water and air and the parameter values are same as those in Section 3.4. Symmetric boundary condition is set at $y=0$m, and outflow conditions are used for other

https://doi.org/10.4208/aamm.2015.m1283 Published online by Cambridge University Press

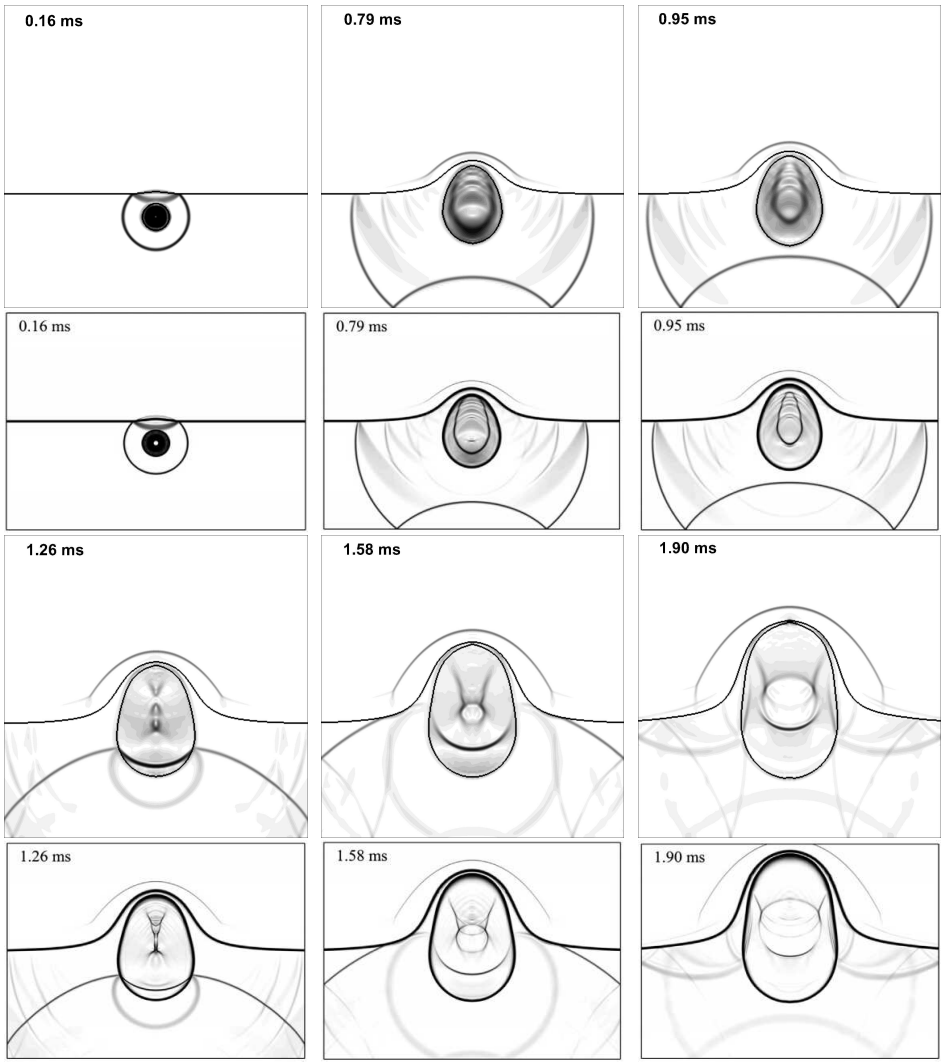


Figure 14: Density schlieren for underwater explosion test case. The first and third rows are present results, second and fourth rows are from Shukla [49]. Current results are obtained with 400×400 cells, and Shukla's results were obtained with 1200×1200 cells.

boundaries.

At the beginning, a high pressure and density bubble interacts with the surrounding water, a circular shock move radially outwards and a rarefaction wave converges to the bubble center. When the shock in water interacts with the ambient water-air interface, a weak shock is formed in ambient air. Figs. 14 and 15 show the evolution of the bubble and the ambient water-air interface, and the present results of density schlieren are compared with Shukla's ones [49] in Fig. 14. The two results are consistent and the interfaces are even clearer in current results, although its grid resolution is much coarser than that

https://doi.org/10.4208/aamm.2015.m1283 Published online by Cambridge University Press

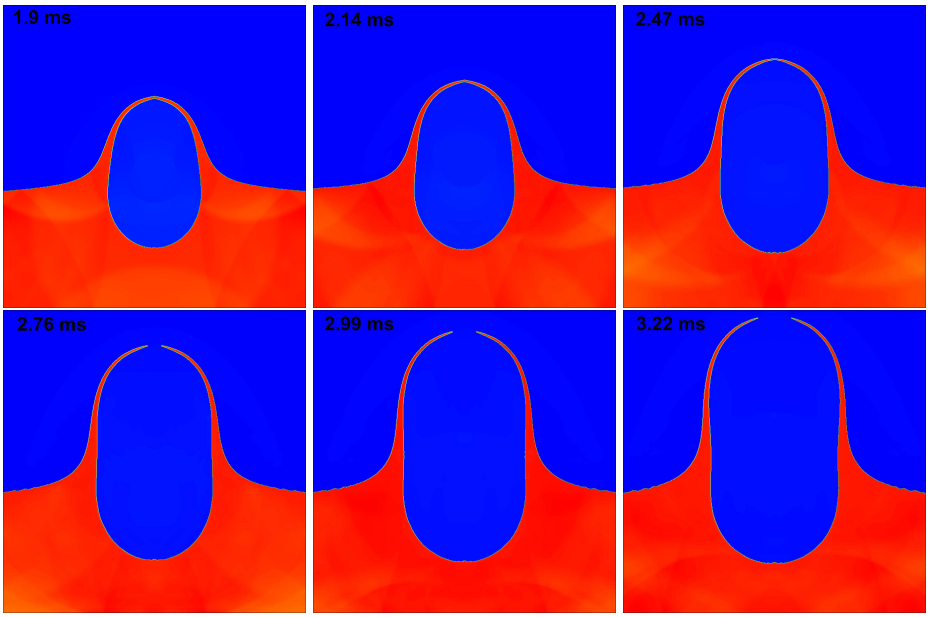


Figure 15: The shape of bubble and interface, after 1.9ms.

in [49], which shows the benefit of sharp interface method.

Fig. 15 shows the shape of bubble and interface after 1.9ms. Present method can capture easily the thin liquid structure between bubble and ambient air until 2.47ms. After that the thin layer will be disconnected and the air bubble will be connected with the ambient air. With this method, not only the fine fluid can be captured (at time 1.90ms, 2.14ms and 2.47ms), but also the disconnection and connection can be treated easily (2.76ms). The density profiles are shown along $x = 2$m at different time in Fig. 16 and compared with Hu et al. [50]. Present results are consistent with their results, with only a small difference at bubble center at time 0.2 ms.

4 Summary and conclusions

In this paper, a new sharp interface method for compressible multi-phase flows is developed, based on the Cut Cell, Level Set and Ghost Fluid method. With LS function, cut points, cut faces and cut cells are calculated, and the velocity of interface is obtained by the exact Riemann solver. The cut cells and nearby regular cells are marked as ghost cells and the states of ghost cells are obtained by the OGFM for gas-gas cases and the GWGFM for air-water cases, so that each of them has both real state of one fluid and ghost state of the other fluid. The states of cell faces are reconstructed by MUSCL scheme and the fluxes are obtained by the AUSM$^+$-up approximate Riemann solver. The conservative quantities on regular cells are updated with a standard finite volume method. The states

https://doi.org/10.4208/aamm.2015.m1283 Published online by Cambridge University Press

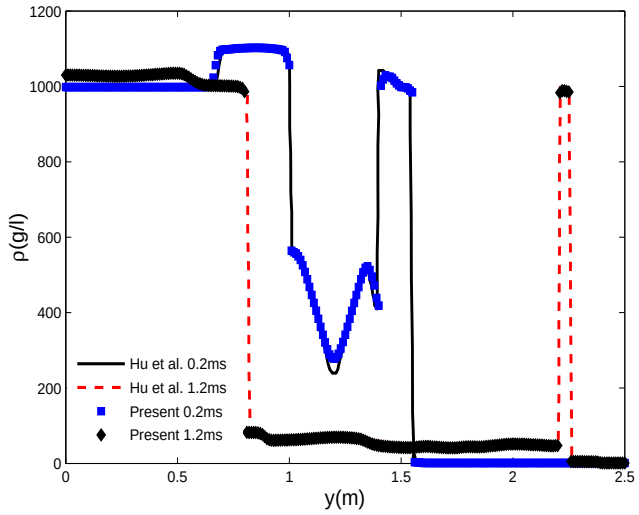


Figure 16: Density profiles of underwater explosion problem along $x=2$m at time 0.2 and 1.2ms. Compared with Hu et al. [50].

of a cell cut by the interface and the related cut cells are calculated and updated by a real-ghost mixing method, which helps to deal with very small cut cells and make the state reconstruction and update uniformly. A cut face reconstruction method similar to volume of fluid is used to reconstruct cut faces in the cells of multiple cuts to deal with topological change.

Various 1D and 2D compressible multi-phase problems are tested to show the ability, accuracy and robustness of current method. It also shows good mass conservation behavior, comparing to some earlier LS method. This method benefits from cut cell in the sharp interface description, and can handle topological change naturally.

Acknowledgments

The authors acknowledge the financial support from National Natural Science Foundation of China (Grant Nos. 11202020, 91230203 and U1530401) and President Foundation of Chinese Academy of Engineering Physics (Grant No. 201501043). We also thank Prof. Hang Ding (USTC) for reading the original manuscript and giving helpful suggestions on the presentation.

References

[1] C. W. HIRT AND B. D. NICHOLS, *Volume of fluid (VOF) method for the dynamics of free boundaries*, J. Comput. Phys., 39 (1981), pp. 201–225.

[2] W. J. RIDER AND D. B. KOTHE, *Reconstructing volume tracking*, J. Comput. Phys., 141 (1998), pp. 112–152.

https://doi.org/10.4208/aamm.2015.m1283 Published online by Cambridge University Press

[3] S. OSHER AND J. A. SETHAIN, *Front propagating with curvature dependent speed: algorithm based on Hamilton-Jaccobi formulation,* J. Comput. Phys., 79 (1988), pp. 12–49.
[4] S. OSHER AND R. P. FEDKIW, *Level Set methods: an overview and some recent results,* J. Comput. Phys., 169 (2001), pp. 463–502.
[5] S. OSHER AND R. P. FEDKIW, Level Set Methods and Dynamic Implicit Surfaces, Springer, 2002.
[6] M. SUSSMAN, E. FATEMI, P. SMEREKA, S. OSHER AND J. A. SETHAIN, *An improved Level Set method for imcompressible two-phase flows,* Comput. Fluids, 27 (1998), pp. 663–680.
[7] D. JACQMIN, *Calculation of two-phase Navier-Stokes flows using phase-field modeling,* J. Comput. Phys., 155 (1999), pp. 96–127.
[8] X. F. YANG, J. J. FENG, C. LIU AND J. SHEN, *Numerical simulations of jet pinching-off and drop formation using an energetic variational phase-field method,* J. Comput. Phys., 218 (2006), pp. 417–428.
[9] I. L. CHERN, J. GLIMM, O. MCBRYAN, B. PLOHR AND S. YANVI, *Front tracking for gas dynamics,* J. Comput. Phys., 62 (1986), pp. 83–110.
[10] J. GLIMM, M. J. GRAHAM, J. GROVE, X. L. LI, T. M. SMITH, D. TAN, F. TANGERMAN AND Q. ZHANG, *Front tracking in two and three dimensions,* Comput. Math. Appl., 35 (1998), pp. 1–11.
[11] R. R. NOURGALIEV, M.-S. LIOU, AND T. G. THEOFANOUS, *Numerical prediction of interfacial instabilities: Sharp interface method (SIM),* J. Comput. Phys., 227 (2008), pp. 3940–3970.
[12] C.-H. CHANG, X. L. DENG AND T. G. THEOFANOUS, *Direct numerical simulation of interfacial instabilities: A consistent, conservative, all-speed, sharp-interface method,* J. Comput. Phys., 242 (2013), pp. 946–990.
[13] R. P. FEDKIW, T. ASLAM, B. MERRIMAN AND S. OSHER, *A non-oscillatory Eulerian approach to interfaces in multimaterial flows (the ghost fluid method),* J. Comput. Phys., 152 (1999), pp. 457–492.
[14] R. CAIDEN, R. P. FEDKIW AND C. ANDERSON, *A numerical method for two-phase flow consisting of separate compressible and incompressible regions,* J. Comput. Phys., 166 (2001), pp. 1–27.
[15] R. P. FEDKIW, *Coupling an Eulerian fluid calculation to a Lagrangian solid calculation with the ghost fluid method,* J. Comput. Phys., 175 (2002), pp. 200–224.
[16] T. G. LIU, B. C. KHOO AND K. S. YEO, *Ghost fluid method for strong shock impacting on material interface,* J. Comput. Phys., 190 (2003), pp. 651–681.
[17] T. G. LIU, B. C. KHOO AND C. W. WANG, *The ghost fluid method for compressible gas-water simulation,* J. Comput. Phys., 204 (2005), pp. 193–221.
[18] C. W. WANG, T. G. LIU AND B. C. KHOO, *A real ghost fluid method for the simulation of multimedium compressible flow,* SIAM J. Sci. Comput., 28 (2006), pp. 278–302.
[19] X. Y. HU AND B. C. KHOO, *An interface interaction method for compressible multifluids,* J. Comput. Phys., 198 (2004), pp. 35–64.
[20] X. Y. HU, B. C. KHOO, N. A. ADAMS AND F. L. HUANG, *A conservative interface method for compressible flows,* J. Comput. Phys., 219 (2006), pp. 553–578.
[21] M. S. LIOU, *A sequel to AUSM: AUSM$^+$-up for all speed,* J. Comput. Phys., 214 (2006), pp. 137–170.
[22] C. H. CHANG AND M. S. LIOU, *A robust and accurate approach to computing compressible multiphase flow: stratified flow model and AUSM$^+$-up scheme,* J. Comput. Phys., 225 (2007), pp. 840–873.
[23] A. JAMESON, *Solution of the Euler equations for two dimensional flow by a multigrid method,* Appl. Math. Comput., 13 (1983), pp. 327–355.

https://doi.org/10.4208/aamm.2015.m1283 Published online by Cambridge University Press

[24] B. P. SOMMEIJER, P. J. VAN DER HOUWEN AND J. KOK, *Time integration of three-dimendional numerical transport models,* Appl. Numer. Math., 16 (1994), pp. 201–225.
[25] R. R. NOURGALIEV AND T. G. THEOFANOUS, *High-fidelity interface tracking in compressible flows: Unlimited anchored adaptived Level Set,* J. Comput. Phys., 224 (2007), pp. 836–866.
[26] H.-K. ZHAO, T. CHAN, B. MERRIMAN AND S. OSHER, *A variational level set approach to multiphase motion,* J. Comput. Phys., 127 (1996), pp. 179–195.
[27] M. SUSSMAN, P. SMEREKA AND S. OSHER, *A Level Set approach for computing solutions to incompressible two-phase flow,* J. Comput. Phys., 114 (1994), pp. 146–159.
[28] M. SUSSMAN, A. S. ALMGREN, J. B. BELL, P. COLELLA, L. H. HOWELL AND M. L. WELCOME, *An adaptive Level Set approach for incompressible two-phase flow,* J. Comput. Phys., 148 (1999), pp. 81–124.
[29] D. P. PENG, B. MERRIMAN, S. OSHER, H. ZHAO AND M. KANG, *A PDE-based fast local Level Set method,* J. Comput. Phys., 155 (1999), pp. 410–438.
[30] R. R. NOURGALIEV, T. N. DINH AND T. G. THEOFANOUS, *Adaptive characteristics-based matching for compressible multifluid dynamics,* J. Comput. Phys., 213 (2006), pp. 500–529.
[31] J. LI, *Calcul d'interface affine par morceaux (Piecewise linear interface calculation),* C. R. Acad. Sci. Paris, Sér. IIb (Paris), 320 (1995), pp. 391–396.
[32] D. L. YOUNGS, *An interface tracking method for a 3D Eulerian hydrodynamics code,* Technical report, AWRE, Technical Report 44/92/35.
[33] R. SAUREL AND R. ABGRALL, *A simple method for compressible multifluid flows,* SIAM J. Sci. Comput., 21 (1999), pp. 1115–1145.
[34] R. D. RICHTMYER, *Taylor instability in shock acceleration of compressible fluids,* Commun. Pure Appl. Math., 13 (1960), pp. 297–313.
[35] E. E. MESHKOV, *Instability of the interface of two gases accelerated by a shock wave,* Fluid Dyn., 43 (1969), pp. 101–104.
[36] E. E. MESHKOV, *Instability of a shock wave accelerated interface between two gases,* NASA Tech. Trans., TT F-13 (1970), pp. 074.
[37] R. L. HOLMES, A Numerical Investigation of the Richtmyer-Meshkov Instability Using Front-Tracking, Ph. D. dissertation, State University of New York at Stony Broke, USA 1994.
[38] R. L. HOLMES, J. W. GROVE AND D. H. SHARP, *Numerical investigation of Richtmyer-Meshkov instability using front-tracking,* J. Fluid Mech., 301 (1995), pp. 51–64.
[39] M. A. ULLAH, W. B. GAO AND D. K. MAO, *Numerical simulations of Richtmyer-Meshkov instabilities using conservative front-tracking method,* Appl. Math. Mech., 32 (2011), pp. 119–132.
[40] P. MOVAHED AND E. JOHNSEN, *A solution-adaptive method for efficient compressible multifluid simulations, with application to the Richtmyer-Meshkov instability,* J. Comput. Phys., 239 (2013), pp. 166–186.
[41] J. F. HAAS AND B. STURTEVANT, *Interaction of weak shock waves with cylindrical and spherical gas inhomogeneities,* J. Fluid Mech., 181 (1987), pp. 41–76.
[42] J. J. QUIRK AND S. KARNI, *On the dynamics of a shock-bubble interaction,* J. Fluid Mech., 318 (1996), pp. 129–163.
[43] M. A. ULLAH, W. B. GAO AND D. K. MAO, *Towards front-tracking based on conservation in two space dimensions III, tracking interfaces,* J. Comput. Phys., 242 (2013), pp. 268–303.
[44] K. M. SHYUE, *A wave-propagation based volume tracking method for compressible multicomponent flow in two space dimensions,* J. Comput. Phys., 215 (2006), pp. 219–244.
[45] H. TERASHIMA AND G. TRYGGVASON, *A front-tracking/ghost-fluid method for fluid interface in compressible flows,* J. Comput. Phys., 228 (2009), pp. 4012–4037.

https://doi.org/10.4208/aamm.2015.m1283 Published online by Cambridge University Press

[46] J. W. GROVE AND R. MENIKOFF, *The anomalous reflection of a shock wave at a material interface,* J. Fluid Mech., 219 (1990), pp. 313–336.
[47] W. BO AND J. W. GROVE, *A volume of fluid based ghost fluid method for compressible multi-fluid flows,* Comput. Fluids, 90 (2014), pp. 113–122.
[48] N. K. BOURNE AND J. E. FIELD, *Shock-induced collapse of single cavities in liquids,* J. Fluid Mech., 244 (1992), pp. 225–240.
[49] R. K. SHUKLA, *Nonlinear preconditioning for efficient and accurate interface capturing in simulation of multicomponent compressible flows,* J. Comput. Phys., 276 (2014), pp. 508–540.
[50] X. Y. HU, N. A. ADAMS AND G. IACCARINO, *On the HLLC Riemann solver for interface interaction in compressible multi-fluid flow,* J. Comput. Phys., 228 (2009), pp. 6572–6589.
[51] J. W. GROVE AND R. MENIKOFF, *The anomalous reflection of a shock wave at a material interface*, J. Fluid Mech., 219 (1990), pp. 313–336.
[52] R. K. SHUKLA, C. PANTANO AND J. B. FREUND, *An interface caputing method for simulation of multi-phase compressible flows,* J. Comput. Phys., 229 (2010), pp. 7411–7439.

https://doi.org/10.4208/aamm.2015.m1283 Published online by Cambridge University Press